Leaky-Wave Antennas Based on Capacitively Tuned Modulated Reactance Surfaces

Anastasios H. Panaretos, *Member, IEEE*, and Douglas H. Werner, *Fellow, IEEE*

***Abstract*—The performance of a leaky-wave antenna that utilizes a sinusoidally modulated reactance surface is numerically investigated. In contrast to previously reported design methodologies, the sinusoidal reactance fluctuation is introduced in the structure by using lumped capacitors that load a frequency selective surface composed of simple uniformly distributed metallic strips. A key advantage of the approach presented herein is that it provides a pathway to realizing a reconfigurable surface impedance by allowing the lumped elements to be tunable. Using a 2-port network representation of the sub-unit-cell, the required capacitance-to-reactance map, necessary to determine the capacitor values that yield the desired sinusoidal reactance profile, can be rapidly extracted.**

***Index Terms*—Capacitance, leaky-wave antennas (LWAs), network theory, periodic structures, surface impedance.**

I. Introduction

In THEIR seminal paper [1], Oliner and Hessel examined the guidance and radiation properties of sinusoidally modulated reactance surfaces. In the context of antenna engineering, their study is of paramount importance because it set the necessary theoretical guidelines required in order to develop a separate class of leaky-wave antennas (LWAs) [2]. This type of antenna is usually composed of frequency selective surfaces (FSSs) etched on a shorted dielectric substrate, where their geometric profile follows some prescribed sinusoidal pattern. More recently, several rather sophisticated LWA designs have been proposed that utilize the concept of modulated reactance surfaces and operate in the microwave regime [3]–[7], or even at THz frequencies [8], [9].

The popularity of modulation reactance surfaces in the development of LWAs stems from the fact that their input impedance can be described in a compact mathematical form. Therefore, as documented in [1], it is mathematically tractable to derive the dispersion relation that governs the radiation and guidance properties of such structures. As a result, given the characteristics of an impedance surface, one can trivially generate the corresponding dispersion diagram, and thus draw conclusions regarding the structure's electromagnetic behavior. Of particular practical importance for the design of LWAs based on modulated impedance surfaces is the work by Patel and Grbic reported in [10]. Through a very informative analysis, they presented a set of guidelines for the design of modulated reactance surface LWAs. Their design realizes the modulated reactance surface through an arrangement of metallic strips etched on a PEC-backed dielectric substrate; the length of the gaps in between these strips follows a prescribed sinusoidal rule. The analysis presented herein to a certain extent parallels the work in [10]. In particular, the possibility is examined for how to realize the modulated reactance properties through lumped capacitors defined across uniformly spaced metallic strips. The success of this attempt is based on the derivation of a realistic capacitance-to-reactance map, similar to the conventional gap-to-reactance map that the modulated strip width based LWA requires. Moreover, the fact that the additional capacitance is introduced in the structure through lumped elements allows the designer to conveniently represent the sub-unit-cell of the reactance surface as a 2-port network. In this way, the necessary loading capacitance, required to achieve the desired sinusoidal profile, is determined through simple and highly efficient circuit computations rather than repetitive time-consuming full-wave simulations as in the case of the modulated strip width-based LWA.

Manuscript received May 26, 2015; revised July 18, 2015 and August 09, 2015; accepted August 12, 2015. Date of publication August 17, 2015; date of current version March 08, 2016. This work was supported in part by a grant from Lockheed Martin.

The authors are with the Electrical Engineering Department, The Pennsylvania State University, University Park, PA 16802 USA (e-mail: tassos@psu.edu; dhw@psu.edu).

Color versions of one or more of the figures in this letter are available online at http://ieeexplore.ieee.org.

Digital Object Identifier 10.1109/LAWP.2015.2469103

II. Devising the Modulated Impedance Surface

For this study, the size of the square unit-cell of the LWA is set equal to 28.25 mm. The structure is composed of 10 identical rectangular sub-unit-cells, each one with a length of 2.825 mm. The FSS of each sub-unit-cell is composed by two PEC strips with size 0.9125×28.25 mm^2 and a 1-mm gap in between them. The FSS is positioned on a shorted dielectric substrate with a thickness of $d = 2.54$ mm. The substrate is composed of Rogers 6006 with $\varepsilon_{\mathrm{r1}} = 6.15 \times (1 - \mathrm{j}0.0019)$. Typically, a modulated impedance surface is realized by allowing the length of the gaps of each sub-unit-cell to vary according to some sinusoidal rule. Essentially, modifying the gap size between the strips corresponds to modifying the equivalent capacitance between the strips. In what follows, a procedure is introduced that describes how to map the properties of a modulated impedance surface onto an equivalent FSS composed of uniformly distributed strips by applying a judiciously chosen nonuniform, sinusoidal, lumped element capacitive loading scheme across the surface (i.e., across each one of the 10 gaps between the sub-unit-cells).

A. Extracting the FSS Admittance

The HFSS computer-aided design (CAD) model of the sub-unit-cell is shown in Fig. 1. As indicated in the figure, the

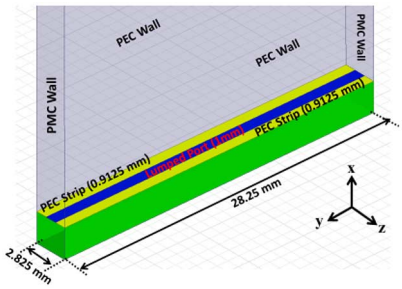

Fig. 1. Sub-unit-cell computational model.

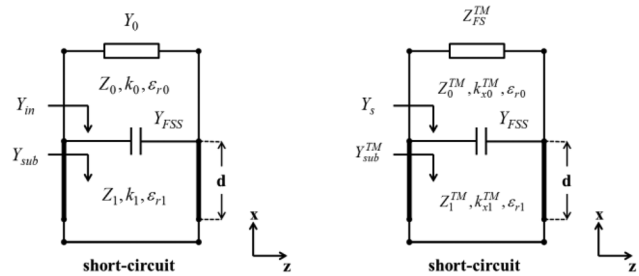

Fig. 2. Circuit equivalent of the sub-unit-cell under (a) TEM and (b) TM excitation.

structure is embedded into a parallel-plate waveguide: The top and bottom faces of the computational domain are defined as PEC boundaries, while the left and right walls are defined as PMC boundaries. The excitation source is a waveguide port with only its TEM mode enabled, de-embedded to the surface of the FSS. In the CAD model, across the 1-mm gap between the two PEC strips, a 50-Ω lumped port is defined that extends across the two PMC walls. This is the most important feature of the numerical setup. In particular, the definition of the lumped port allows the excited sub-unit-cell to be represented as a 2-port network: Port #1 is the excitation waveguide port, while port #2 is the lumped port. Therefore, by performing a single full-wave simulation, the corresponding 2×2 S-parameter matrix can be extracted. Now, for any load $Z_{\rm L}$ applied across the lumped port, the reflection coefficient at port #1 can be trivially obtained using the following formula [11]:

$$\Gamma_{\rm in} = S_{11} + \frac{S_{12}S_{21}\Gamma_{\rm L}}{1 - S_{22}\Gamma_{\rm L}}. \tag{1}$$

In (1), the S_{ij} terms are obtained from the full-wave simulation mentioned previously, while $\Gamma_{\rm L}$ is the reflection coefficient created when the desired load $Z_{\rm L}$ is used to terminate a transmission line with characteristic impedance 50 Ω. In conclusion, by utilizing (1), it is possible to compute the reflection coefficient of the sub-unit-cell for any applied capacitive loading $Z_{\rm L}$, without having to run repetitive full-wave simulations.

The importance of (1) stems from the convenience it offers to very rapidly extract the admittance of the FSS for any loading scenario. In particular, with respect to the circuit equivalent model shown in Fig. 2(a), the admittance of the FSS can be expressed as

$$Y_{\rm FSS} = Y_{\rm in} - Y_{\rm sub} \tag{2}$$

where $Y_{\rm sub}$ is the input admittance of the PEC backed substrate given by

$$Z_{\rm sub} = Y_{\rm sub}^{-1} = jZ_1 \tan(k_1 d) = j\frac{Z_0}{\sqrt{\varepsilon_{\rm r1}}} \tan\left(\frac{\omega}{c_0}\sqrt{\varepsilon_{\rm r1}}d\right) \tag{3}$$

and c_0 is the speed of light in free space. The input admittance of the structure $Y_{\rm in}$ is given by

$$Y_{\rm in}^{-1} = Z_{\rm in} = Z_0\frac{1+\Gamma_{\rm in}}{1-\Gamma_{\rm in}} \tag{4}$$

where $\Gamma_{\rm in}$ is obtained from (1) and $Z_0 = 377\ \Omega$.

B. Reactance-to-Capacitance Map

In the next stage of this analysis, a methodology is developed in order to represent a prescribed modulated surface impedance profile, through nonuniform capacitively loaded sub-unit-cells. First, the corresponding TM input admittance of the capacitively loaded FSS sub-unit-cell shown in Fig. 2(b) is obtained, which is given by

$$Y_s = Z_s^{-1} = Y_{\rm FSS} + Y_{\rm sub}^{\rm TM} = Y_{\rm FSS} + \frac{1}{jZ_1^{\rm TM}\tan(k_{x1}^{\rm TM}d)}. \tag{5}$$

In the preceding expression, $Y_{\rm FSS}$ is obtained from (2). Also, $Y_{\rm sub}^{\rm TM}$ is the TM admittance of the shorted substrate, where $Z_1^{\rm TM} = k_{x1}^{\rm TM}(\omega\varepsilon_0\varepsilon_{\rm r1})^{-1}$ is the corresponding TM characteristic impedance. Application of the transverse resonance technique along the interface between free space and the loaded sub-unit-cell geometry, as shown in Fig. 2(b), yields

$$Z_{\rm FS}^{\rm TM} + Z_s = 0 \Rightarrow \frac{k_{x0}^{\rm TM}}{\omega\varepsilon_0} = -Z_s \tag{6}$$

where the TM expression for the free-space impedance $Z_{\rm FS}^{\rm TM}$ has been utilized. Now, by subtracting the dispersion relations that govern the propagation of TM waves in the two media (free space/sub-unit-cell), we obtain

$$\left(\frac{k_{x1}^{\rm TM}}{k_0}\right)^2 - \left(\frac{k_{x0}^{\rm TM}}{k_0}\right)^2 = \varepsilon_{\rm r1} - 1 \tag{7}$$

which can be further simplified with the aid of (6) as

$$\left(\frac{k_{x1}^{\rm TM}}{k_0}\right)^2 - \left(\frac{Z_s}{Z_0}\right)^2 = \varepsilon_{\rm r1} - 1. \tag{8}$$

The next step is to determine a numerical solution to the system of (5) and (8). To accomplish this, we first let $Z_s = {\rm j}X$, where the reactance X is assumed to vary from 0 Ω to 2 kΩ, and then search for the value of Z_s that satisfies (5) subject to the condition in (8).

Before proceeding further with the analysis, it is instructive to demonstrate the accuracy of (1) in determining the reflection coefficient from the sub-unit-cell for different capacitive loading scenarios. Fig. 3(a) shows comparisons of the reflection coefficient phase resulting from the capacitively loaded sub-unit-cell as computed using (1) and through full-wave simulations. As seen from this comparison, the responses predicted by the two

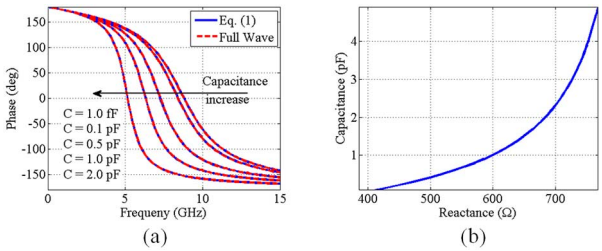

Fig. 3. (a) Reflection coefficient comparisons for different sub-unit-cell capacitive loadings. (b) Reactance-to-capacitance map.

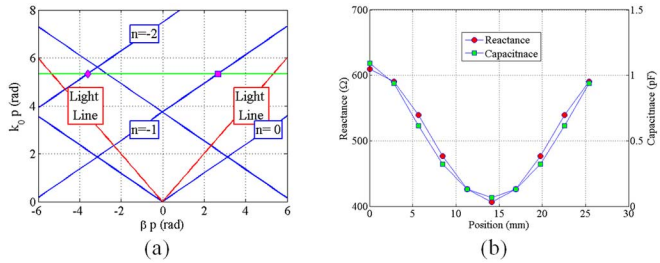

Fig. 4. (a) Dispersion diagram. (b) Reactance-to-capacitance map for a modulated impedance surface.

methods are in excellent agreement. Note here that the 1.0-fF capacitor load essentially corresponds to an unloaded sub-unit-cell. It should be mentioned here that (2) and (3) are valid if the substrate thickness d is large enough so that higher-order coupling effects between the metallic strips and the ground plane can be neglected. For the structure under study, this condition is satisfied as indicated by the validation results shown in Fig. 3(a).

Having verified the accuracy of the FSS impedance retrieval methodology based on (1), we proceed with the extraction of the loading capacitance/sub-unit-cell impedance map. For this reason, we let the loading capacitance vary discretely as follows $[0.001, 0.002 : 0.1 : 5] \times 1$ pF. Next, using (1) and (2), the impedance of the loaded FSS is derived, and finally from (5) and (8), the TM input impedance of the sub-unit-cell is computed. The resulting reactance-to-capacitance map that can be achieved from this particular sub-unit-cell configuration is shown in Fig. 3(b). Based on this correspondence, in what follows the desired modulated surface impedance profile is translated into equivalent capacitors and the radiation properties of the LWA are engineered accordingly.

III. Numerical Results

The impedance profile of a general modulated impedance surface is given by [1]

$$Z_s(z) = jX_{\mathrm{s}}\left[1 + M\cos\left(\frac{2\pi z}{p}\right)\right] \tag{9}$$

where M is the modulation factor, p is the unit-cell length, and X_{s} is the average surface reactance. For the LWA under consideration, the modulation factor is set equal to $M = 0.2$, and it is desired to achieve radiation at $\theta_{n=-1} = 30°$, at $f_0 = 9$ GHz. Note here that the modulation factor in principle can have any value less than one. However, in this example, the value of M was chosen so that the resulting surface impedances are mapped to realistic lumped capacitor values as shown in Fig. 3(b). According to the design methodology described by Patel and Grbic in [10], the average reactance of the modulated impedance surface is equal to

$$\frac{X_{\mathrm{s}}}{Z_0} = \sqrt{-1 + \left(\sin\theta_{n=-1} + \frac{c_0}{f_0 p}\right)^2}. \tag{10}$$

For the case examined here, (10) yields $X_{\mathrm{s}} = 1.35Z_0$. The corresponding dispersion diagram, based on these design specifications, is shown in Fig. 4(a). Note that the depicted dispersion diagram does not exhibit stopbands; this is because we have purposely considered the dispersion diagram that corresponds to an unmodulated surface impedance (i.e., $M = 0$). The dispersion relation for this case is given by

$$\beta = k_0\sqrt{1 + \left(\frac{X_{\mathrm{s}}}{Z_0}\right)^2} \tag{11}$$

which provides reliable information as long as the frequency range of interest does not coincide with the locations of the stopbands. It should be emphasize that the aforementioned design procedure is valid provided that the modulation factor is small. If this is not the case, (11) fails to accurately predict the propagation constant, and thus the direction of the main lobe will be squinted [1], [10].

The green horizontal line shown in Fig. 4(a) denotes all the wave-vectors that correspond to 9 GHz. It can be seen that there is a major radiating lobe at the intersection of the 9-GHz line with the $n = -1$ harmonic, and a minor lobe at its intersection with the $n = -2$ harmonic, denoted with the square and the rhombic marker, respectively. The radiation angle of the minor lobe is around $\theta_{n=-2} = -43°$.

For the chosen modulation factor, the maximum and minimum values of the surface's reactance are $X_{\mathrm{s}} \times (1 + M) = 610\ \Omega$ and $X_{\mathrm{s}} \times (1 - M) = 407\ \Omega$, respectively. The objective now is to generate 10 equidistant, with respect to space, sinusoidally varying reactance values that fluctuate within the aforementioned minimum and maximum values. For this reason, we evaluate the impedance in (9) at the sequence of points: $z_k = \frac{p}{10}k$, with $k = 0 : 1 : 9$. Then, these reactance values are mapped to capacitances, with the resulting correspondence graphically depicted in Fig. 4(b). The set of lumped capacitor loads required for application across the 10 sub-unit-cells in order to achieve radiation at 30° were determined to be: [0.9382, 0.6145,0.3211,0.1323, 0.0673, 0.1323, 0.3211, 0.6145,0.9382, 1.0943] $\times$ 1 pF.

The HFSS CAD model developed to test the performance of the capacitively tuned reactance modulated surface-based LWA is shown in Fig. 5. The antenna consists of 10 unit-cells excited by parallel-plate waveguides (PPWs). Note that the metallic strips are uniformly spaced, however the aforementioned nonuniform lumped capacitor loading scheme is used to achieve the required effective impedance modulation. Also, note that the side walls of the bounding box of the computational model are defined as PMCs, while the top, front, and rear walls are assigned a radiation boundary condition.

Fig. 6(a) displays the realized gain of the LWA as a function of elevation angle. Moreover, the realized gain for five different

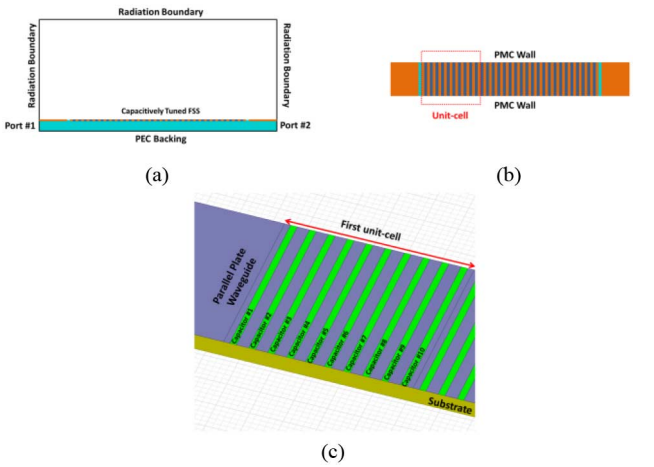

Fig. 5. LWA computational model. (a) Side view. (b) Top view. The actual LWA consists of 10 unit-cells. A shorter version of the LWA consisting of only 3 unit-cells is shown in order to facilitate a better image of the geometrical details. (c) Zoomed-in image of the actual HFSS CAD model showing the capacitor arrangement for each sub-unit-cell comprising the first unit cell of the LWA.

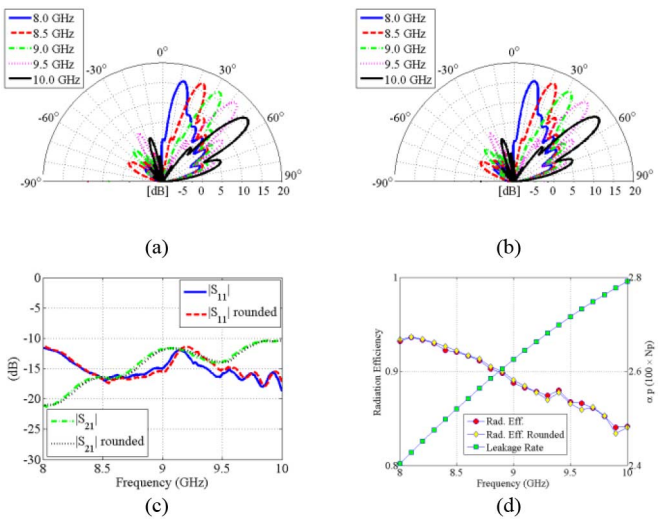

Fig. 6. (a) Realized gain. (b) Realized gain based on commercially available capacitors. (c) S_{11} and S_{21}. (d) Radiation efficiency and leakage rate.

frequencies is indicated in the legend of the figure. First, it can be seen that the desired main radiation lobe at 9 GHz is slightly squinted and directed to $32.5°$, while as also predicted, the secondary minor lobe radiates towards $-42°$ (left semicircle). Furthermore, it can also be seen that as the operating frequency of the antenna sweeps from 8 to 10 GHz, its major lobe monotonically scans from $10°$ to $50°$. Fig. 6(b) displays the realized gain of the LWA as a function of elevation angle when the lumped capacitors are rounded to commercially available values, namely $[0.9, 0.6, 0.3, 0.1, 0.1, 0.1, 0.3, 0.6, 0.9, 1.1] \times 1$ pF. It can be clearly seen that the LWA retains its radiation properties. The S_{11} and S_{12} performances for this LWA configuration for the actual and rounded lumped capacitor loads are shown in Fig. 6(c). Finally, Fig. 6(d) shows the radiation efficiency of the two LWAs along with the leakage rate computed as described in [1].

IV. Conclusion

We have numerically demonstrated the operating principles of an LWA that utilizes a sinusoidally modulated reactance surface. Contrary to conventional approaches, the FSS comprising the LWA does not follow a sinusoidal geometric pattern, but rather the sinusoidal reactance fluctuation is introduced using lumped capacitors that load an arrangement of uniformly distributed metallic strips. The proposed methodology provides a compact approach towards the synthesis of electronically tunable LWA antennas, with agile beam-scanning capabilities. Moreover, the loading scheme introduced here is not limited to impedance surfaces composed of uniform unit-cells. It can just as easily be applied to impedance surfaces composed of nonuniform unit cells. This would allow, for example, nonuniform sinusoidally modulated LWAs to be engineered such that the resulting amplitude and phase distribution across the aperture could be readily controlled [12].

References

[1] A. A. Oliner and A. Hessel, "Guided waves on sinusoidally-modulated reactance surfaces," *IRE Trans. Antennas Propag.*, vol. AP-7, no. 5, pp. 201–208, Dec. 1959.

[2] A. A. Oliner and D. R. Jackson, "Leaky-wave antennas," in *Antenna Engineering Handbook*, J. L. Volakis, Ed., 4th ed. New York, NY, USA: McGraw-Hill, 2007.

[3] B. Fong, J. Colburn, J. Ottusch, J. Visher, and D. Sievenpiper, "Scalar and tensor holographic artificial impedance surfaces," *IEEE Trans. Antennas Propag.*, vol. 58, no. 10, pp. 3212–3221, Oct. 2010.

[4] G. Minatti, F. Caminita, M. Casaletti, and S. Maci, "Spiral leaky-wave antennas based on modulated surface impedance," *IEEE Trans. Antennas Propag.*, vol. 59, no. 12, pp. 4436–4444, Dec. 2011.

[5] S. Maci, G. Minatti, M. Casaletti, and M. Bosiljevac, "Metasurfing: Addressing waves on impenetrable metasurfaces," *IEEE Antennas Wireless Propag. Lett.*, vol. 10, pp. 1499–1502, 2011.

[6] G. Minatti, S. Maci, P. De Vita, A. Freni, and M. Sabbadini, "A circularly polarized isoflux antenna based on anisotropic metasurface," *IEEE Trans. Antennas Propag.*, vol. 60, no. 11, pp. 4998–5009, Nov. 2012.

[7] S. K. Podilchak, L. Matekovits, Al. P. Freundorfer, Y. M. M. Antar, and M. Orefice, "Controlled leaky wave radiation from a planar configuration of width-modulated microstrip lines," *IEEE Trans. Antennas Propag.*, vol. 61, no. 10, pp. 4957–4972, Oct. 2013.

[8] J. S. Gómez-Díaz, M. Esquius-Morote, and J. Perruisseau-Carrier, "Plane wave excitation-detection of non-resonant plasmons along finite-width graphene strips," *Opt. Exp.*, vol. 21, pp. 24 856–24 872, 2013.

[9] M. Esquius-Morote, J. S. Gómez-Díaz, and J. Perruisseau-Carrier, "Sinusoidally-modulated graphene leaky-wave antenna for electronic beam-scanning at THz," *IEEE Trans. Terahertz Sci. Technol.*, vol. 4, no. 1, pp. 116–122, Jan. 2014.

[10] A. M. Patel and A. Grbic, "A printed leaky-wave antenna based on a sinusoidally modulated reactance surface," *IEEE Trans. Antennas Propag.*, vol. 59, no. 6, pp. 2087–2096, Jun. 2011.

[11] D. Pozar, *Microwave Engineering*, 3rd ed. Hoboken, NJ, USA: Wiley, 2005.

[12] A. J. Martínez-Ros, J. L. Gómez-Tornero, V. Losada, F. Mesa, and F. Medina, "Non-uniform sinusoidally modulated half-mode leaky-wave lines for near-field focusing pattern synthesis," *IEEE Trans. Antennas Propag.*, vol. 63, no. 3, pp. 1022–1031, Mar. 2015.